NANO LETTERS
Cite This: Nano Lett. 2018, 18, 6931−6940
Letter
pubs.acs.org/NanoLett

Nanodroplet Hydrodynamic Transformation of Uniform Amorphous Bilayer into Highly Modulated Ge/Si Island-Chains

Yaolong Zhao,[†] Haiguang Ma,[†] Taige Dong,[†] Junzhuan Wang,[†] Linwei Yu,*[,†,‡] Jun Xu,[†] Yi Shi,[†] Kunji Chen,[†] and Pere Roca i Cabarrocas[‡]

[†]National Laboratory of Solid State Microstructures/School of Electronics Science and Engineering/Collaborative Innovation Center of Advanced Microstructures, Nanjing University, 210093 Nanjing, China

[‡]LPICM, CNRS, Ecole Polytechnique, Université Paris-Saclay, 91128 Palaiseau, France

Supporting Information

ABSTRACT: Geometric and compositional modulations are the principal parameters of control to tailor the band profile in germanium/silicon (Ge/Si) heteronanowires (NWs). This has been achieved mainly by alternating the feeding precursors during a uniaxial growth of Ge/Si NWs. In this work, a self-automated growth of Ge/Si hetero island-chain nanowires (hiNWs), consisting of wider c-Ge islands connected by thinner c-Si chains, has been accomplished via an indium (In) droplet-mediated transformation of uniform amorphous a-Si/a-Ge bilayer thin films. The surface-running In droplet enforces a circulative hydrodynamics in the nanoscale droplet, which can modulate the absorption depth into the amorphous bilayer and enable a single-run growth of a superlattice-like hiNWs without the need for any external manipulation. Meanwhile, the separation and accumulation of electrons and holes in the phase-modulated Ge/Si superlattice leads to a modulated surface potential profile that can be directly resolved by Kelvin probe force microscopy. This simple self-assembly growth and modulation dynamics can help to establish a powerful new concept or strategy to tailor and program the geometric and compositional profiles of more complex hetero nanowire structures, as promising building blocks to develop advanced nanoelectronics or optoelectronics.

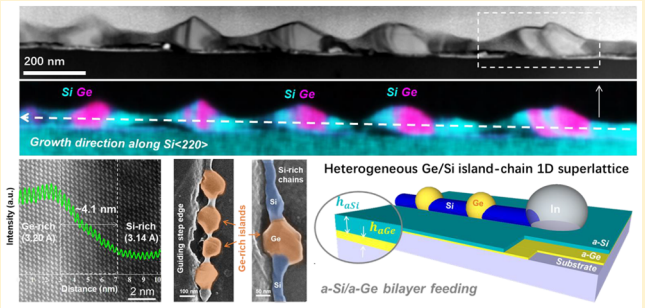

KEYWORDS: *Ge/Si hetero nanowires, nanodroplet hydrodynamics, self-assembly growth*

The ability to modulate the compositional profile in germanium (Ge) and silicon (Si) superlattice structures has been the key to achieve artificially designed electronic, photonic, and phononic properties and functionalities.[1−3] The band profile engineering becomes more prominent in quasi one-dimensional (1D) Ge/Si superlattice nanowires (NWs),[3−12] where both a stronger lateral confinement and a periodic diameter variation can contribute to an enhanced band profile and transport modulation in the 1D channels. So far, periodic diameter modulations in Ge or Si NWs are usually accomplished by top-down electron beam lithography[13,14] and selective etching.[15,16] While compositional modulations in hetero Ge/Si NWs are mostly fabricated by vertical etching into a planar Ge/Si superlattice,[4,17] self-assembly growth led by nanometal droplets represents a straightforward, economic, and versatile bottom-up approach[18−20] to engineer the composition in Ge/Si NWs,[5−9,21−25] where the precursor supplies are alternated periodically during a vapor−liquid−solid (VLS)[5−9,21,22] or a solution−liquid−solid[23−25] growth process. In these precursor-alternating approaches, the chamber or solution environment has to be evacuated completely twice to complete a single period of Ge/Si segments to guarantee a thoroughly compositional transition and minimize the reservoir effects (for VLS growth, in the catalyst metal droplets).[8,9,26] This leads to a rather slow sequential multistep control to engineer the superlattice-like Ge/Si hetero NWs. Particularly, long intervals are usually required to purge the preceding atoms to suppress the reservoir effect or by using alloy metal catalyst with a rather low solubility of Si and Ge atoms[22] and reducing the growth temperature.[5,21] In view of all these challenges in the external control, there arises an interesting question: is it possible to appoint the catalyst droplets alone to accomplish such a self-modulation of NWs in terms of their composition or/and geometry profiles?

So far, a single-run growth of Ge/Si NW superlattices with interlaced Ge-rich and Si-rich segments has not been possible without the aid of external parametric controls. Though periodic c-Ge islands can be formed directly upon the sidewall of c-Si NWs, via a postgrowth Plateau-Rayleigh transformation of the outer amorphous germanium (a-Ge) shell,[27,28] the c-Si

Received: July 12, 2018
Revised: October 14, 2018
Published: October 22, 2018

DOI: 10.1021/acs.nanolett.8b02847
Nano Lett. 2018, 18, 6931−6940

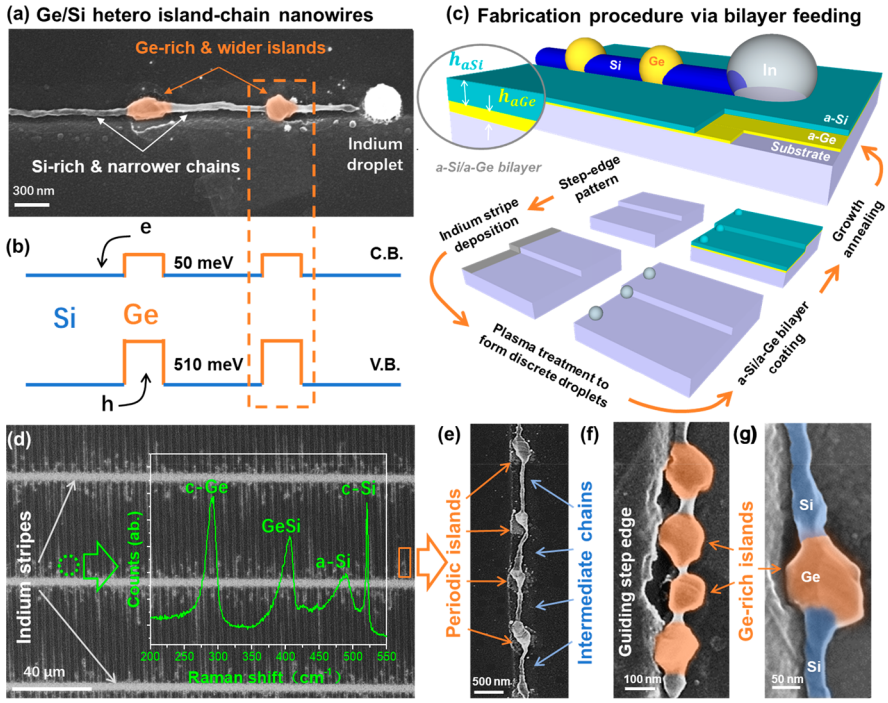

Figure 1. Morphologies and fabrication procedures of Ge/Si hetero island-chain nanowires (hiNWs). (a) SEM image of a typical Ge/Si hiNW with Ge-rich island (wider in brown) and Si-rich chain (narrower in gray) structure, grown by an In droplet. (b) Schematic sketches of the type-II band alignment among crystalline Ge-rich islands and Si-rich chains.[29,30] The main fabrication steps of the in-plane Ge/Si hiNWs, guided along step edges with amorphous a-Si/a-Ge bilayer feeding, are illustrated in (c). (d) A Raman spectrum of the selected region of the Ge/Si hiNWs in the region marked by the dashed green circle. (e–g) Closer SEM characterizations of the Ge/Si hiNWs, grown along the guiding step edges with varying diameters and island-to-island spacing.

NW cores remain continuous and unchanged. In contrast to the above-mentioned precursor feeding-sequence controls, we here propose a fundamentally different stack-sequence control that exploits nanoscale molten indium (In) droplets to accomplish an automatic selective absorption of stacked a-Si (top)/a-Ge (bottom) bilayers to produce Ge/Si hetero island-chain nanowire (hiNW) superlattices. Specifically, molten In droplets can be employed to develop a unique hydrodynamics under proper bilayer thickness ratio that leads to a periodic selective absorption of the a-Si/a-Ge bilayer to produce highly modulated hiNWs with a significant compositional and geometric modulation, as seen for example in the scanning electron microscope (SEM) image shown in Figure 1a. This compositional modulation opens the opportunity to engineer a unique band profile in hetero nanowires, as depicted schematically in Figure 1b, which could provide a solid basis for developing more complex and potentially more functional photonic or optoelectronic device applications.

The in-plane hiNWs were grown upon glass or oxide-coated c-Si substrates, via an in-plane solid–liquid–solid (IPSLS) mechanism,[31−38] as diagrammed in Figure 1c. For example, discrete In droplets were first formed by a hydrogen plasma treatment in a plasma-enhanced chemical vapor deposition (PECVD) system, and then covered with a-Si (top)/a-Ge (bottom) bilayer at ∼150° (below the melting point of In). This was followed by an annealing at 300° that activated the droplets to absorb the amorphous bilayer precursor and deposit crystalline hiNWs behind. In order to control the growth direction of hiNWs, step edges were etched into the substrate to provide guiding lines. More experimental details and the guiding growth mechanism are described in Experimental Section and our previous works.[37,39,40] A typical SEM image of a single Ge/Si hiNWs, grown from left to right along a step edge, is shown in Figure 1a, where the brighter spot at the end of the hiNW is the leading In droplet. In strong contrast with the previous in-plane growth studies with a single a-Si layer as precursor,[31,33] both the bilayer stack sequence and their relative thickness ratio provide the major control parameters to stimulate a floating-dwelling absorption dynamics leading to a self-automated geometric and compositional modulation in the Ge/Si hiNWs.

Figure 1d–g provides a close scrutiny of the Ge/Si hiNWs, which were grown by In droplets starting from the prepatterned In stripes, identified in Figure 1d as the horizontal bright lines and guided by a parallel array of step edges in vertical directions. Remarkably, the Ge/Si hiNWs feature a series of wide island nodes with narrow chain segments in between. Pseudocolors are applied in Figure 1e,g to highlight the large diameter modulation and compositional phase separation among the island and chain regions, which were produced by nano In droplets in a single run self-assembly growth. Note that for the specific sample in Figure 1d, the yield of guided growth of island-chain Ge/Si NWs is found to be ∼70%, estimated by sampling 50 different places along the guiding edges. A larger SEM view of the guided Ge/Si hiNWs is also provided in Figure S1, accompanied by four different zoom-in SEM images of the local hiNW structures. Raman characterization (Horiba Jobin-Yvon operated at 514 nm incident light in a backscattering configuration at normal incidence) of the Ge/Si hiNW arrays, recorded over a large region marked by the dashed green circle in the Figure 1d, reveals several peaks, corresponding to the composition of c-Si, a-Si, c-Ge, and SiGe alloy at 520, 480, 290, and 410 cm^{-1}, respectively, indicating that the a-Si/a-Ge bilayer has been

DOI: 10.1021/acs.nanolett.8b02847
Nano Lett. 2018, 18, 6931−6940

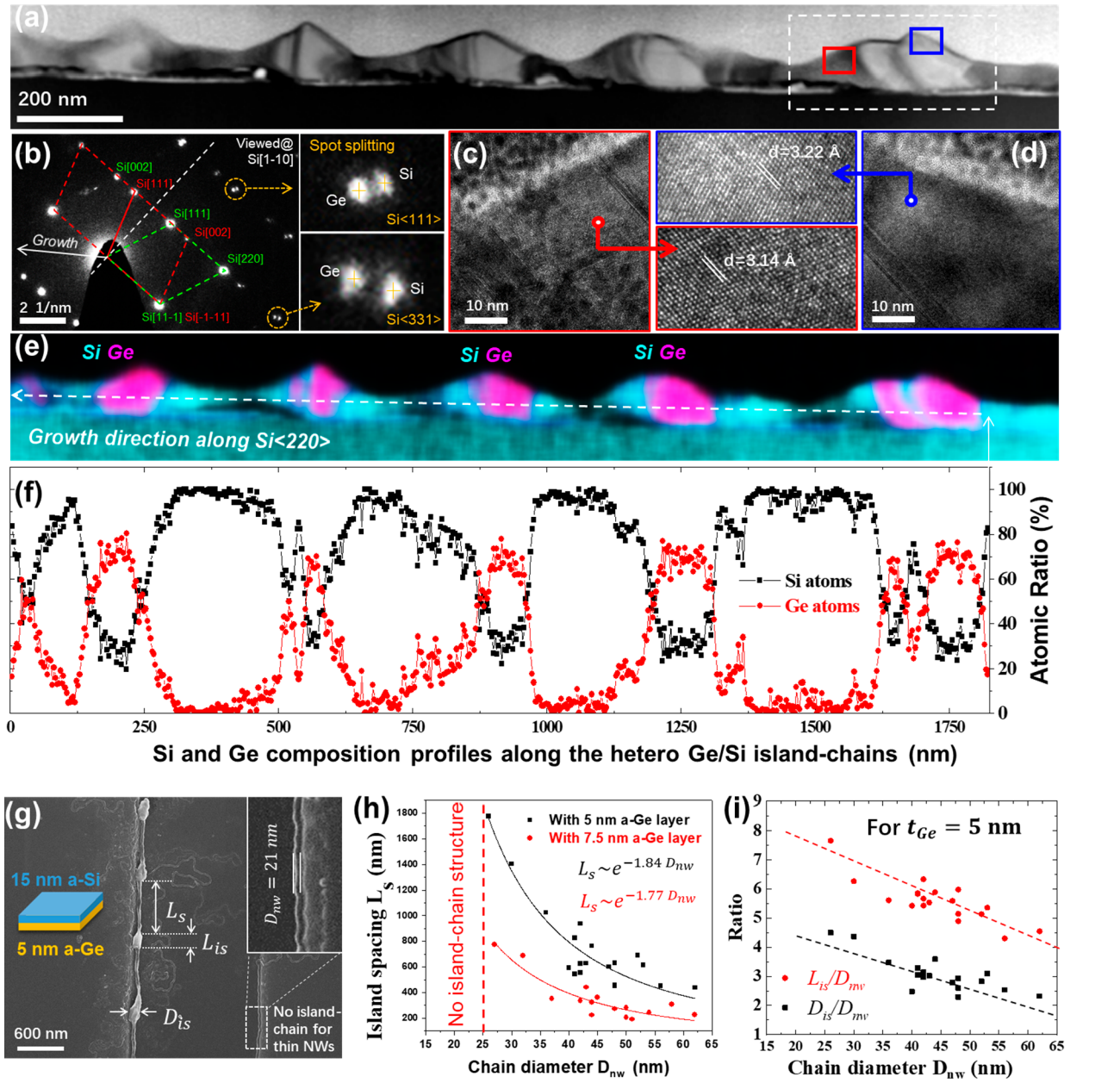

Figure 2. (a) A TEM characterization of an in-plane Ge/Si hiNW. A SAD pattern of the region, as marked by the white dashed rectangle, is displayed in (b), where the spot splitting in Si ⟨111⟩ and Si ⟨331⟩ directions are highlighted in the two insets on the right. Scale bars in (a–d) stand for 200 nm, 2 nm^{-1}, 10 nm, and 10 nm. Closer high-resolution TEM examinations of the lattice fringes in two distinct regions on the opposite sides of the phase-separated boundary as indicated by the red and blue squares are presented in (c,d), respectively. The EDS elemental mapping along the hiNW is presented in (e), where the Si and Ge elemental mapping are overlapped and labeled by cyan and pink colors, respectively. The Si and Ge composition profile is extracted and plotted in (f), along the growth direction of Si ⟨220⟩. SEM image in (g) reveals that the thicker and the thinner hiNWs, grown from the same a-Si (15 nm)/a-Ge (5 nm) bilayer, develop different geometries. The evolution of the island-to-island spacing L_s, as well as the ratios of the island diameter D_{is} and the island length L_{is} over the chain diameter, are extracted and plotted in (h,i), as a function of different chain diameter D_{nw}.

converted into an array of hiNWs consisting of interlaced c-Ge and c-Si regions.[41]

The structural properties and compositional variation of the Ge/Si hiNWs were further examined by using high-resolution transmission electron microscopy (HR-TEM) analysis and electron dispersive spectroscopy (EDS) element mapping, as shown in Figure 2a,e, respectively. The side-view HRTEM image of a hiNW segment, which is cut and transferred to a copper grid by focused ion beam milling and with the help of nanomanipulators, reveals a series of distinctive Ge/Si hetero island-chain structures with significant diameter variations, coupled with a regular and highly modulated Ge/Si compositional alternation. The c-Ge segments are identified as the brighter and wider islands in the dark-field TEM imaging due to their higher density compared to that of the c-Si phase. This is confirmed by the elemental mapping of the Ge (pink) and Si (cyan) atom distributions, displayed and overlapped in Figure 2e, while more elemental mapping analysis is provided in Figure S2, where a thin layer of remnant a-Ge can be usually found just below the narrow c-Si chain segments. According to

DOI: 10.1021/acs.nanolett.8b02847
Nano Lett. 2018, 18, 6931−6940

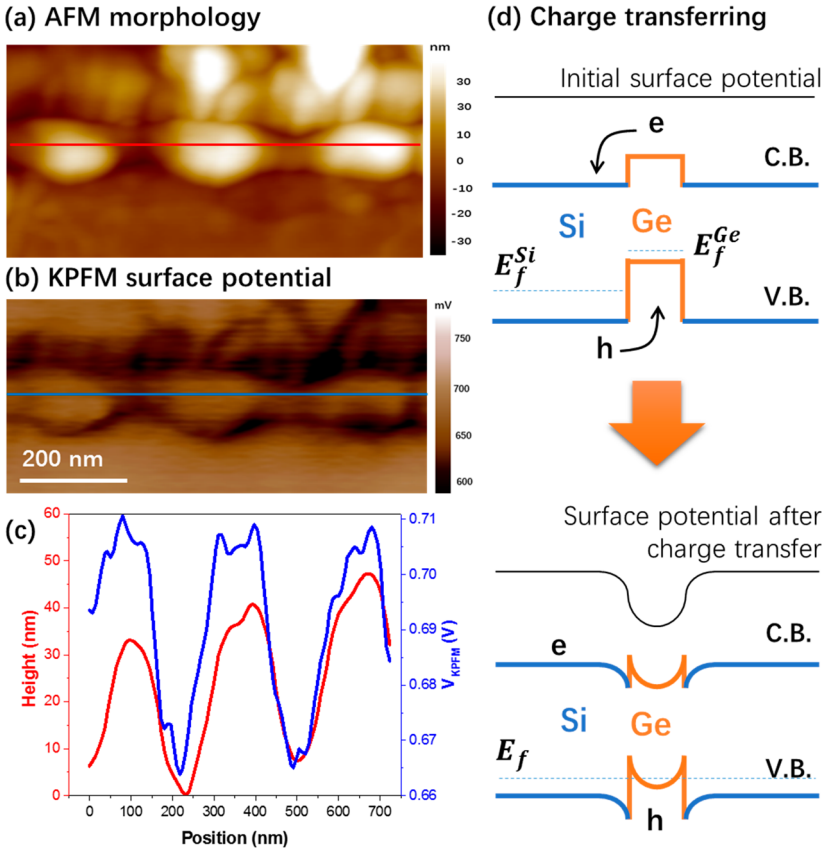

Figure 3. (a,b) The geometry and static potential profiles obtained via AFM and KPFM analysis, respectively, while the extracted height (red) and potential (blue) variation profiles, along the corresponding scan lines in (a,b), are presented in (c). (d) Schematic sketches of the origin of the surface potential variations due to the electrons and holes separation at the Ge (island)/Si (chain) hetero interface with a type-II band offset. C.B. and V.B. stand for conduction band and valence band, respectively.

the Ge/Si profile plot in Figure 2f, which is extracted along the hiNW (from right to left), sharp Si-to-Ge phase transitions are found at the onsets of the two right-most islands, where the narrower Si-rich (>98%) chain is switched quickly into the formation of bulky Ge-rich islands. Though the EDS analysis of the sliced sample could not provide a 3D reconstruction of the phase-separation in the Ge-rich islands, the local EDS profile captured in Figure 2f does confirm that there is a clear and sharp Ge/Si phase transition happens over an interface of <10 nm in the island, accompanied by significant Ge content increase rising from basically 0% to almost 75%. Then, at the end of the growth of Ge-rich islands, the diameter shrinks gradually, accompanied by a phase transition back to the c-Si in the narrower chains. Occasionally, a high-frequency compositional alternation (with layer thickness <20 nm) can be found within the wider island regions. Selected area diffraction (SAD) analysis (Figure 2b) of a selected island-chain unit, as delimitated by the white dashed lines in Figure 2a, discloses a diffraction pattern that reveals a different lattice spacing among the c-Ge islands and the c-Si chains with a lattice mismatch of 2.6% estimated according to the diffraction spot splitting in ⟨111⟩ and ⟨331⟩ directions (highlighted in the insets to the right of Figure 2b).[42] This is also consistent with the HR-TEM lattice fringe imaging of the Si-rich (marked by the red rectangle in Figure 2a) and the Ge-rich (blue) regions, shown in Figure 2c,d with corresponding lattice spacing of 3.14 and 3.22 Å, respectively. In addition, according to Vegard's law and experimental verification,[43] the GeSi alloy with 75% Ge content should have a lattice constant of 5.596 Å, corresponding to a $Si_{[111]}$ lattice spacing of 3.23 Å, which agrees well with the measured value in Figure 2d. This finding indicates that the Ge-rich region in the wide island segments exist as uniform $Ge_{0.75}Si_{0.25}$ alloy. Meanwhile, Figure 2f also shows that the maximal Ge concentrations detected in the different islands are all of ∼75%, which also implies that the Ge-rich segments are composed of uniform GeSi alloy phase with a similar Ge concentration, instead of overlapping phase-separated Ge and Si segments stacked in the TEM observation direction.

Meanwhile, it is also worth to note that the phase transition interfaces of the two left-most islands in Figure 2f is found to be less sharp compared to those in the two right-most islands. This could result from a slight growth orientation change of the Ge/Si hiNWs, which caused a misalignment of these interfaces with respect to the HR-TEM observation direction, which was focused to be parallel to the interface planes in the two right-most islands. As a consequence, the abruptness of the tilted interfaces could be smeared off. In order to evaluate the actual interface abruptness, the interfaces in the second island (count from left) were re-examined by using aberration-corrected HRTEM and high-angle annular dark-field scanning transmission electron microscopy (HAADF-STEM), as shown in Supporting Figure S3. According to the intensity profile extracted and plotted in Figure S3b, across the interface in the region marked by the red square in Figure S3c the transition interface has a width of ∼4.1 nm, whereas the average spacing measured on the left and the right-hand sides of the interface is 3.20 and 3.14 Å, corresponding to the Ge-rich and the Si-rich

DOI: 10.1021/acs.nanolett.8b02847
Nano Lett. 2018, 18, 6931−6940

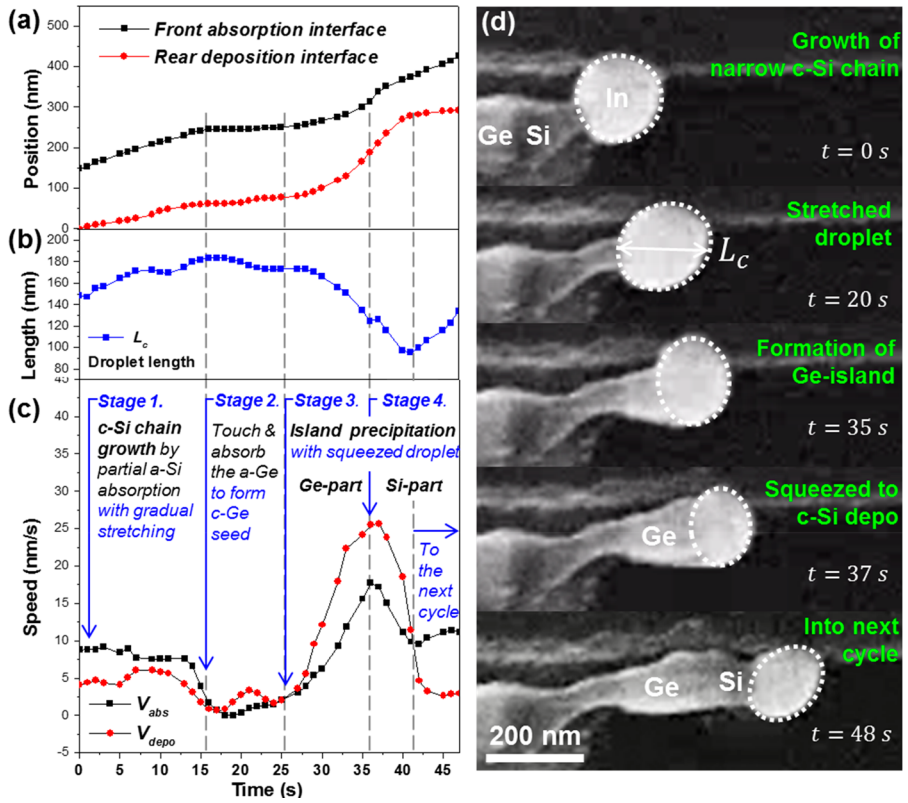

Figure 4. (a) The temporal evolution of the positions of the front absorption and the rear deposition interfaces of a moving In droplet during a complete growth cycle of the island-chain heterostructure with a series of snapshots taken by in situ SEM observation at different times shown in (d). The scale bar in (d) is for 200 nm. The derived catalyst length and the moving rates of the front the rear interfaces are extracted and presented in (b,c), respectively.

regions. This is also consistent with the HAADF-STEM analysis presented in Figure S3d, where the green and the red spots stand for Ge and Si atoms, respectively. It is also important to note that, as the EDS mapping shown in Figure 2 has been carried out on a sliced island-chain Ge/Si NW sample with a thickness of only ∼60 nm, it is not possible at this moment to reconstruct a comprehensive 3D picture of the phase separation interface within the Ge-rich island zones. Our future work will continue to investigate this interesting aspect by means of more advanced 3D EDS analysis on complete island-chain structures. In the meantime, the In element mapping is also carried out and presented in Figure S3e, where the In signals are mostly detected as the remnant spots or traces around the hiNW structure, for example, the brighter spot found in the left-bottom corner of Figure S3c.

The impact of the highly modulated compositional variation in the Ge/Si hiNWs was investigated by using Kelvin probe force microscopy (KPFM) characterization (Oxford Instrument, carried out in ambient air at room temperature of 25° with a relative humidity of RH = 30%; the tip−sample distance was kept at 10 nm with a AC bias of 0.6 V), which is capable of revealing the local surface potential variation among heterostructures.[44] The atomic force microscope (AFM) profilometry and the corresponding KPFM potential (V_{KPFM}) mapping of a selected region, comprising three islands, are shown in Figure 3a,b, respectively. According to the extracted height and V_{KPFM} potential displayed in Figure 3c, the Ge-rich islands correspond to the regions with a higher V_{KPFM} potential signal (of $\delta V \sim 45$ mV) with respect to their neighboring Si-rich chains. In addition, KPFM scanning on a reference pure Si NWs sample did not reveal any surface potential variation. Similar to the carriers separation observed in core−shell Ge/Si NWs,[45] the holes and electrons in this axial Ge/Si heterostructure are separated at the Ge/Si interface, due to a type-II Ge/Si band offset, as depicted schematically in Figure 3d. As a consequence, the accumulated holes (electrons) in the Ge-rich islands (Si-rich chains) cause a higher (lower) electrostatic potential. Meanwhile, during the in-plane growth, In catalyst atoms will be incorporated into the in-plane NWs to give a p-type doping in the c-Si.[40,46] A similar p-type doping effect has also been documented for the substitutional incorporation of In atoms into the c-Ge matrix, which will introduce a level lying only 11 meV above the valence band top, compared to the deeper doping level of In atoms lying 160 meV above the valence band top in c-Si.[30] Thus, the major charge migration among the hiNWs involves the transfer of holes from the Si-rich chains to the Ge-rich islands. Meanwhile, it is important to note that the KPFM characterization operating with a nulling-DC-bias mechanism[44] is basically insensitive to the local geometric capacitance. Though the measured V_{KPFM} potential values here cannot provide quantitative assessments of the actual potentials (because of the existence of moisture), their relative variation trend is, irrespective of the environmental moisture (at least in a range of RH = 0% to 60%),[47] and can therefore provide a meaningful and informative clue to infer the local surface potential variation resulting from the band profile modulation and carrier separation in the phase-separated Ge/Si hiNWs.

Interestingly, the formation dynamics of such hiNWs can be observed directly via an in situ SEM characterization, where

DOI: 10.1021/acs.nanolett.8b02847
Nano Lett. 2018, 18, 6931−6940

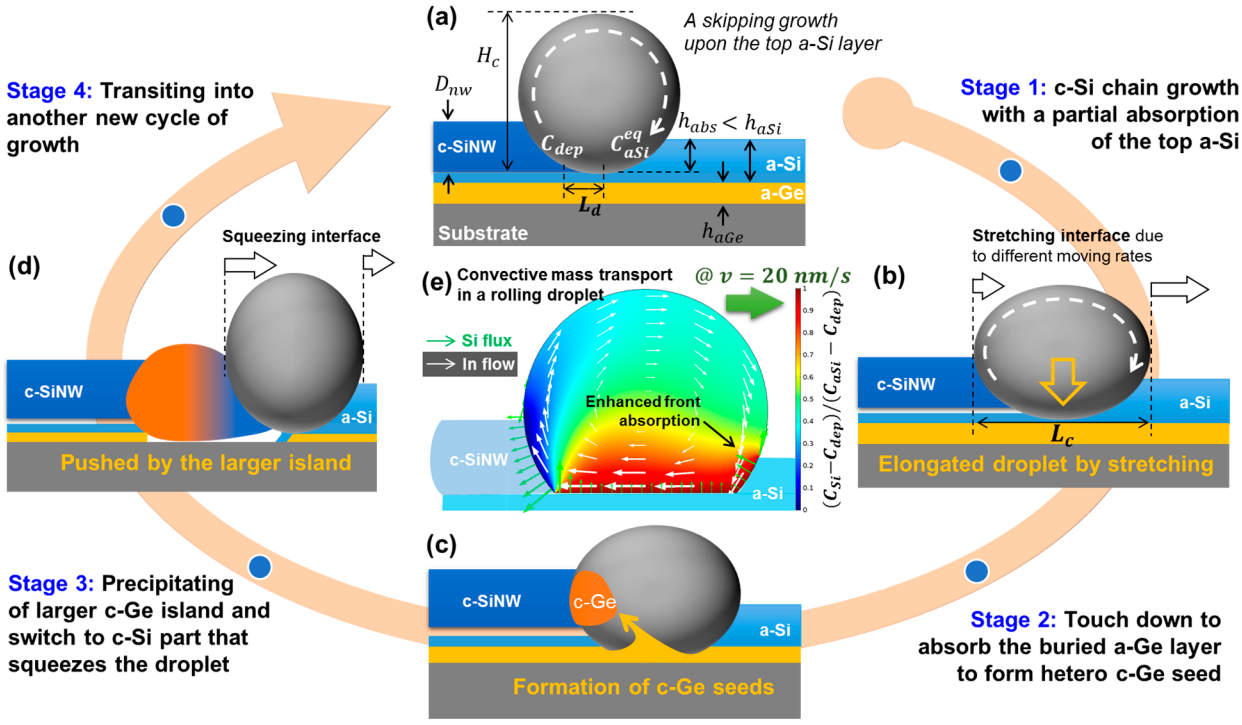

Figure 5. (a–d) Schematic illustrating the skipping growth, interface stretching, hetero island formation and interface squeezing dynamics happening during a complete growth cycle, whereas (e) presents a simulated convective mass transport of dissolved Ge or Si atoms in a rolling forward In droplet.

the sample after amorphous bilayer coating was transferred from the PECVD system to the SEM chamber equipped with a heating stage (more details are provided in the Experimental Section). The in-plane growth can be activated in vacuum upon heating to 300°, which is sufficient to melt the droplets to absorb the a-Si/a-Ge bilayer. In this way, the temporal evolution of the positions of the front absorption and the rear deposition interfaces (see Figure 4a) can be recorded, according to the SEM snapshots taken at different time steps shown in Figure 4d. A remarkable finding is that the geometry and the growth rate of In droplets are not constant. As inferred from the temporal variations of the catalyst length L_C and the interface moving rates in Figure 4b,c, respectively. There are four distinct growth stages that can be identified, during a complete growth cycle of the island-chain unit. They include, as indicated in Figure 4c:

Stage 1. The growth of a c-Si narrow chain, where the In droplet consumes only a part of the top a-Si layer, with a large catalyst droplet (D_c)-to-nanowire (D_{nw}) diameter contrast $f = D_{nw}/D_c$. During this stage, the droplet is found to be gradually stretched by the front and the rear interfaces, because the former is moving at a higher rate than the latter.

Stage 2. The In droplet slows down quickly and almost comes to a stop, while the top a-Si layer is completely consumed to expose the bottom a-Ge layer, triggering a fast absorption of Ge atoms into the droplet.

Stage 3. A rapid precipitation of a wider and brighter c-Ge island out of the In droplet that pushes and squeezes the In droplet quickly to accelerate with the rear deposition interface moving 40% faster than the front absorption interface.

Stage 4. Finally, the moving rates of both interfaces turn to decrease steadily but still the faster running rear interface with respect to the front one continues to squeeze the In droplet into ~60% of its origin length at the end of this stage. After that, the droplet is observed to rebound and speed up again, into the skipping and stretching stage in the next growth cycle, as indicated in Figure 4c.

The periodic stretching and squeezing dynamics of the In droplets, accompanied by growth rate variation, provides a critical clue to infer the internal hydrodynamics taking place within the running In droplet. First of all, it is important to note that the different growth rates of the front absorption (v_{abs}) and the rear deposition (v_{dep}) interfaces can deform the In droplet and stimulate a rich hydrodynamics. Second, to form a Ge/Si hiNW, the droplet is supposed to develop a skipping growth dynamics, during the growth of the narrower c-Si chain, as illustrated in Figure 5a, where the top a-Si layer is only partially absorbed, not touching the buried a-Ge layer. This situation has been indeed observed experimentally, as shown in Figure S4, where the in-plane SiNWs grown with a partial a-Si layer absorption ($h_{abs} < h_{aSi}$) can be easily distinguished from their darker trench regions covered with remnant a-Si layer, compared to the brighter trenches for the thicker SiNWs grown by larger droplets with a complete a-Si absorption. Meanwhile, the partial a-Si layer absorption (during a skipping or floating stage) also reduces significantly the diffusion distance, L_d, measured from the a-Si/In absorption interface to the deposition In/SiNW interface from roughly the length of In droplet ($L_d \sim L_c$ in complete absorption case) to extremely small value, as explained and illustrated with more details in Figure S5. This also means that the Si concentration at the rear deposition interface C^{par}_{dep} in partial a-Si absorption can be much higher than that in complete absorption case $C^{cm}_{dep} < C^{par}_{dep}$ and approaching to the equilibrium concentration at the In/a-Si interface $C^{par}_{dep} \rightarrow C^{eq}_{aSi}$.

During the in-plane growth on a solid substrate, the nonsliding bottom liquid/substrate interface is also supposed to enforce a rolling forward hydrodynamics in the droplet.

DOI: 10.1021/acs.nanolett.8b02847
Nano Lett. 2018, 18, 6931–6940

While the absorption and mass transport of Si atoms is driven by a diffusion flux from the In/a-Si interface (with a high equilibrium Si concentration of C_{aSi}^{eq}) toward the rear depositing interface (with a lower concentration of C_{dep}), the convective circulation in a running In droplet, as depicted in Figure 5a by the white dashed arrow, can largely modify the mass transport and Si absorption flux distribution along the In/a-Si absorption interface. For example, as shown in the simulated mass transport in a moving droplet in Figure 5e, this circulation can bring the low Si concentration flow, just passing the deposition interface, to flush directly the front absorption interface, in the clock-wise convective circulation path (Figure 5a), which thus promotes the forward absorption of the front a-Si layer. In the meantime, this clockwise circulation also accumulates a high Si concentration flow over the bottom In/a-Si interface, which can, to some extent, suppress the vertical absorption of the bottom a-Si layer. As shown in the Figure S6, a higher moving rate will favor a more selective absorption of the a-Si layer in the lateral direction ($v_l = v_{abs}$), against that in the vertical direction (v_v). When, on average, it is satisfied that

$$\tau_l \equiv \frac{L_c}{v_l} < \tau_v \equiv \frac{h_a}{v_v} \tag{1}$$

the In droplet will be able to carry out a skipping in-plane growth, that is, without a complete absorption of the underlying a-Si layer.

Meanwhile, there is always a mass conservation constraint on the in-plane growth, which requires that the absorption flux from the front interface has to be balanced by the rear deposition flux, which can be formulated as follows

$$f^2 H_c D_c v_{dep} = \alpha h_a D_c v_{abs} \rightarrow \frac{v_{dep}}{v_{abs}} = \frac{\alpha}{f^2}\frac{h_a}{H_c} \tag{2}$$

where $\alpha \sim 0.9$ stands for the volume contraction ratio between a-Si and c-SiNW[48] and $f = \frac{H_{nw}}{H_c} = \frac{D_{nw}}{D_c}$ a geometric constant related to the interface/surface tension balance at the triple-phase-line.[31,33,36] For a floating growth, the effective absorption depth into the a-Si layer is reduced, as $h_{abs} < h_a$, due to the inner circulation. This will, according to eq 2, lead to a slowdown in the rear deposition interface, and consequently an effective interface stretching, as illustrated schematically in Figure 5b. A stretched droplet with a larger L_c will, as stated in eq 1, increase the lateral traveling time and cause a deeper absorption into the a-Si layer. If this trend continues to an extent sufficient to consume the whole a-Si layer, the buried a-Ge layer will be exposed and get absorbed quickly into the In droplet, as schematically shown in Figure 5c. The equilibrium solubility of Ge atoms in In liquid is actually 3 orders of magnitude higher, $C_{cGe}^{eq} = 2.4$ atom %, than that of Si atoms, which is only $C_{cSi}^{eq} = 3.2 \times 10^{-3}$ atom % at the growth temperature of 350°.[49,50] Therefore, the thin a-Ge layer (5−10 nm in this work) under the In droplet can be quickly absorbed into the In droplet, for instance, the In droplet of D_c = 300 nm seen in Figure 1a, without reaching a supersaturation, $S_{Si(Ge)} \equiv C_{dep}^{Si(Ge)}/C_{cSi(cGe)}^{eq}$. This will encourage a vertical absorption, sinking and even spreading of the In droplet, in order to reach more a-Ge layer, causing a wider pit around the islands as seen in the SEM images in Figure 1a,e.

In parallel, the sudden replenishment of Ge into the In droplet also boosts the supersaturation state of the dissolved Si atoms, according to the ternary phase diagram of In−Ge−Si,[51] and thus the dissolved Si atoms will precipitate even more quickly. This also suppresses the absorption of more Si from the front In/a-Si interface, as witnessed in Figure 4c, where the front interface moving rate v_{abs} drops to near zero in Stage 2. During this dwelling interval, a supersaturation of Ge atoms is eventually achieved in the In droplet, and then a stable hetero nucleus of c-Ge seed can be formed at the end of the c-Si chain. As Ge atoms have a much higher solubility compared to Si atoms, $C_{cGe}^{eq}/C_{cSi}^{eq} > 10^3$,[49,50] the precipitation of Ge atoms can proceed at a much higher rate, $v_{dep}^{Ge} \gg v_{dep}^{Si}$, as the rate is proportional to the absolute concentration of Si or Ge atoms at the deposition interface, $v_{dep}^{Si(Ge)} \sim C_{Si(Ge)}$. This enables a rapid deposition switching from Si to Ge, usually observed at the onset of the islands with a local high compositional contrast of Ge/(Ge + Si) ratio >75%, as witnessed in Figure 2e. An even higher local Ge/(Ge + Si) elemental contrast of 98% was observed in another cross section analysis and EDS mapping of a different island-chain hiNW grown along Si ⟨111⟩ orientation and at a slightly lower temperature of 290°, as shown in Figure S7. The formation of a wider c-Ge island with respect to that of c-Si chain can be assigned to the different surface and interface tension balance condition at the triple-phase-line on the newly formed Ge segment. Similar phenomena have been reported in Si-to-Ge segment transition in solution environment[23−25] and in feeding-gas-modulated VLS growth.[9]

When the bottom a-Ge layer is gradually consumed, the Ge concentration starts to decrease, which equivalently reduces the supersaturation state of dissolved Si[51] that encourages now taking in more Si atoms from the front In/bilayer interface. As a consequence, the droplet starts to move again, corresponding to the transition observed from Stage 2 to Stage 3 in Figure 5c. On the other hand, this initial kicking off is also pushed by the formation of a larger island node behind, which can force the droplet to advance. However, during this initial acceleration, that is, before the speed becomes high enough to carry out a floating growth (as in the case in Stage 1), both the top a-Si and the bottom a-Ge layers are absorbed together. So, a c-GeSi alloy phase will appear during this transition stage with gradually decreasing Ge phase toward pure Si phase in the chain, as seen for example in the tails of the right-most two islands in Figure 2a and Figure S7. Meanwhile, high-frequency interlacing c-Ge and c-Si segments are also found in the transition region of the islands, as witnessed in Figure 2a and Figure S3. This could be assigned to the instable initial kicking off during the acceleration of the droplet, which could experience some fluctuations that cause the droplet to float (upon the a-Si layer) only for a while, and then retouch the buried a-Ge (under the short course of new advancement) again, leaving alternating slices of c-Si and c-Ge in the tail transition region. Eventually, when the droplet gains enough speed to float upon (and absorb only) the top a-Si layer, the in-plane growth switches to the formation of pure and narrower c-Si chain in the next Ge/Si hetero island-chain cycle.

It is critical to note that the bilayer stacking sequence of a-Si (top)/a-Ge (bottom) is a prerequisite to stimulate such self-modulated nanodroplet hydrodynamics to translate the amorphous bilayer into Ge/Si hiNW superlattice. Reversing the bilayer sequence to a-Ge(top)/a-Ge(bottom) or to a uniform amorphous a-GeSi alloy thin film as precursor produces only continuous but basically uniform GeSi alloy NWs, as seen in the Figure S8. Furthermore, with the right bilayer sequence the thickness control of the a-Si and a-Ge sublayers can play a key role in tuning the island-chain

DOI: 10.1021/acs.nanolett.8b02847
Nano Lett. 2018, 18, 6931−6940

geometry and spacing. For example, the evolution of the island-to-island spacing L_s, the diameter D_{is}, and the length L_{is} of the island nodes (as indicated in Figure 2g), as functions of the c-Si chain diameters (D_{nw}) are extracted and displayed in Figure 2h,i, respectively. In the case of tiny NWs (with D_{nw} < 25 nm, led by small In droplets), only uniform and tiny c-Si NWs will grow without apparent island-chain geometry (see the right one in Figure 2g for example). This is because the leading catalyst droplets are simply too small to eat through the top a-Si layer and thus a continuous floating growth will produce pure c-Si NWs. Then, for the hiNWs with a larger chain diameter of D_{nw} > 25 nm the island-chain self-modulation emerges with an island-to-island spacing L_s decreasing monotonically with thicker D_{nw} (that is, grown by larger droplets). A similar scaling trend is observed for both a-Ge layer thicknesses (t_{Ge} = 5 or 7.5 nm) as witnessed in Figure 2h, which can be fitted by a power law of $L_s \sim e^{-1.8\, D_{nw}}$ in a range of 25 nm < D_{nw} < 65 nm. Meanwhile, the geometric ratio of the lengths and the diameters of the island nodes to the chain diameter, that is, the ratios of L_{is}/D_{nw} and D_{is}/D_{nw}, also decreases linearly with larger D_{nw}, as shown in the statistics in Figure 2i.

There are two mechanisms that could account for such scaling trends. First, with a larger liquid droplet the rotation frequency in the rolling In droplet, $f_{roll} \sim D_c/v_{abs}$, will decrease, which will reduce the efficiency or contribution of the circulated mass transport in the droplet. Thus, this will undermine the very basis for sustaining a skipping growth dynamics upon the top a-Si layer, as illustrated in Figure 5, making it easier for the droplet to "eat" through the top a-Si layer and to trigger an island formation (upon touching/absorbing the bottom a-Ge layer). Second, a larger droplet will require a larger amount of a-Si or a-Ge to replenish, as the volume scales with $\sim D_c^3$ while the supplies underneath increases by $\sim D_c^2 h_{aSioraGe}$. This also reduces the equilibrium concentration of Si or Ge atoms in the droplet that will favor a deeper a-Si layer absorption to expose the underlying a-Ge layer. Meanwhile, as seen in Figure 2i, the diameter variation of the Ge-rich islands decreases steadily with thicker D_{nw}, reflecting that the incremental contribution of the a-Ge layer is gradually neutralized in large In droplets. A thicker a-Ge layer seems to increase the dwelling time of the droplet with deeper vertical absorption that could also slow down the moving rate of the droplets. However, the detailed mechanism for that remains to be better understood in future investigations. It is also important to note that as the growth balance condition is related to and determined by the ratio of the catalyst size over the thickness of the provided a-Ge/a-Si bilayer, it is thus in principle possible to scale the Ge/Si hiNWs to be even thinner in diameter and shorter in island spacing by reducing the bilayer thickness (but keeping constant ratio) in proportion to the use of smaller leading In droplets. To give an example, Figure S9 presents the SEM image of a Ge/Si hiNW grown out of a thinner amorphous bilayer stack of 10 nm a-Si (top)/5 nm a-Ge (bottom) with 10 nm initial indium thickness. The diameter of the narrow Si segments measures only 20 nm, while the apparently deeper and darker pits formed around the wider islands are caused by a droplet-skipping growth dynamics that periodically dips into the a-Si/a-Ge bilayer to absorb the bottom a-Ge layer and form the larger Ge-rich islands.

Meanwhile, the relatively rough surface observed on the Ge/Si hiNWs, with respect to the VLS grown vertical SiNWs, could be caused by the significant interface interaction dynamics during such a low temperature growth at only 300−350°, as well as the step-edge roughness or random fluctuations on the substrate surface. To get a smoother sidewall morphology control, one could adjust the growth balance condition, as stated in eq 2, to avoid too much squeezing interface interaction and droplet distortion, or adopt smoother guiding edge and cleaner substrate surface to minimize the environmental roughness perturbation. In parallel, growth-temperature control plays also an important role in tailoring the growth rate and geometry of the Ge/Si hiNWs; this is also constrained by the needs of a sufficiently high temperature to ensure a fast and smooth growth and the caution to avoid spontaneous self-crystallization of the buried a-Ge layer at an elevated temperatures (for instance, >400°). We found that slightly decreasing of the growth temperature to 290° can lead to a higher Ge/Si contrast but also much rougher hiNW sidewalls, as witnessed in the HR-TEM and EDS mapping shown in Supporting Figure S7.

In addition, in view of achieving a high quality real time record of the Ge/Si island-chain growth and formation dynamics, in situ TEM observation with STEM-EDX analysis tool will be very helpful to develop key and unambiguous understandings and theory on the detailed mechanism of the self-automated Ge/Si phase transition. However, this will also necessitate a delicate and more challenging growth of the Ge/Si hiNWs directly upon a very thin (typically <200 nm) and fragile suspended thin film substrate, for instance, of SiN_x to allow the transmitted electron imaging in HR-TEM mode. Hopefully, this kind of advanced characterization will become available in our future works, so as to shed more light on this peculiar hetero Ge/Si island-chains growth dynamics.

In summary, a novel self-automated droplet skipping−dwelling growth hydrodynamics has been witnessed that can be explored to transfer simple a-Si/a-Ge bilayer control into highly modulated in-plane Ge/Si island-chain heteronanowires superlattice. A rapid and self-automatic and propagating compositional transition has been observed among the Ge-rich island and Si-rich chain segments, with a tunable geometry control by the bilayer stack sequence and thicknesses without the need for any external intervention. Meanwhile, it is also important to note that this spontaneous and significant geometry and composition self-modulation in the Ge/Si hiNW heterostructures represents a new and general framework that could be applied to engineer other alloy or compound semiconducting materials. This is highly valuable to promote potential interdisciplinary applications built upon the key capability of bandgap and geometric tailoring in heterostructured NW channels.

Experimental Section. *Substrate Patterning.* The in-plane GeSi NWs are grown on glass substrates or c-Si(100) wafers covered with a 300 nm oxide layer, which were cleaned using standard RCA procedures prior to experiments. The parallel guiding edges were patterned by etching of 150 nm into the underlying SiO_2 layer by photolithography and subsequent reactive ion etching (RIE). The In stripes, lying perpendicular to and crossing the guiding edge lines as depicted in Figure 1c, were deposited by lithography patterning and thermal evaporation.

Indium Droplet Formation. The sample was loaded into the chamber of a plasma-enhanced chemical vapor deposition (PECVD) system, where a H_2 plasma treatment is applied at 300° with 100 SCCM flow rate, 100 Pa chamber pressure, and

DOI: 10.1021/acs.nanolett.8b02847
Nano Lett. 2018, 18, 6931−6940

125 mW/cm^2 RF power density. During this process, the surface In_2O_3 oxide layer on the In strips was reduced and the In thin film was allowed to melt and agglomerate into discrete droplets.

Stacked a-Si/a-Ge Bilayer Deposition. a-Ge:H or a-Si:H layers were deposited separately at a temperature of 150°. The a-Ge layer is deposited by 10 SCCM H_2-diluted (90%) GeH_4 plasma in a PECVD chamber for 75 to 150 s with 80 Pa chamber pressure and 50 mW/cm^2 RF power density, whereas the subsequent a-Si:H layer was deposited by the decomposition of 10 SCCM pure SiH_4 in the plasma with 60 Pa pressure and 60 mW/cm^2. In this work, the a-Si:H layer thickness is fixed to 15 nm, while the thickness of the underlying a-Ge:H layer is varied from 5 to 7.5 nm. Note that a reference sample with opposite bilayer stack sequence was also prepared for comparison.

Ge/Si Nanowire Growth. Upon raising the substrate temperature to 350° in vacuum, the In droplets melt and started to move laterally by absorbing the nearby amorphous bilayers to produce crystalline Ge/Si heterostructures. Thanks to an unique guiding growth mechanism,[40] most of the hetero NWs grew along the guiding edge lines of etched SiO_2 steps, as seen in the SEM image in Figure 1d−1f because the extra amorphous coating on the step sidewall can help to effectively attract the lateral movement of the In droplets.

In Situ SEM Observation. For in situ SEM observation, a 1 cm^2 square piece of c-Si wafer was prepared with the same procedure, as described above in the PECVD system, up to the step of a-Si/a-Ge coating. Then, the sample was unloaded and transferred to a SEM system (Zeiss Sigma) equipped with a heating stage (Kammrath & Weiss GmbH, Heating Module 800 °C). During the transferring, the sample was kept in a low-vacuum box, and the total air-exposure duration is controlled to be <5 min. According to the device manual and the engineers' explanation, the heating region is surrounded and isolated by several concentric layers of reflective, high-temperature resistant sheet metal, and the heating effect on such a small piece of sample is basically uniform with a temperature variation estimated to be <5°. When the stage is heated to 300° (displayed temperature) in the SEM chamber, the In droplets start to move around by absorbing the amorphous bilayer to produce Ge/Si hiNWs.

■ ASSOCIATED CONTENT

Supporting Information

The Supporting Information is available free of charge on the ACS Publications website at DOI: 10.1021/acs.nanolett.8b02847.

SEM Zoom-in details of Ge/Si hiNWs; morphology and elemental mapping; HR-TEM characterization of a sharp Ge/Si transition interface; in-plane growth with complete or partial a-Si layer absorption; illustration for the growth balance condition; simulation of the convective mass transport in a rolling droplet; Ge/Si hiNWs grown at lower temperature; GeSi alloy nanowires grown with reverse stack sequence; Ge/Si hiNWs with thinner bilayer feeding led by smaller droplets (PDF)

■ AUTHOR INFORMATION

Corresponding Author

*E-mail: yulinwei@nju.edu.cn.

ORCID

Linwei Yu: 0000-0002-0801-5210

Pere Roca i Cabarrocas: 0000-0003-2241-2762

Notes

The authors declare no competing financial interest.

■ ACKNOWLEDGMENTS

The authors acknowledge the financial support from the State Key Research Program of the National Natural Science Foundation of China under Grant 021013002006, National Basic Research 973 Program under 2014CB921101, NSFC under 61674075 and 61735008, the Jiangsu Excellent Young Scholar Program under BK20160020, Jiangsu Shuangchuang Team's Personal Program, and the Fundamental Research Funds for the Central Universities. The authors are also grateful to Prof. X. Wang and Dr. B. Wu for their kind support in KPFM characterization and discussion.

■ REFERENCES

(1) Brunner, K. *Rep. Prog. Phys.* **2002**, *65* (1), 27.
(2) Pearsall, T. P.; Bevk, J.; Feldman, L. C.; Bonar, J. M.; Mannaerts, J. P.; Ourmazd, A. *Phys. Rev. Lett.* **1987**, *58* (7), 729−732.
(3) Amato, M.; Palummo, M.; Rurali, R.; Ossicini, S. *Chem. Rev.* **2014**, *114* (2), 1371−412.
(4) Hu, M.; Poulikakos, D. *Nano Lett.* **2012**, *12* (11), 5487−5494.
(5) Wen, C.-Y.; Reuter, M. C.; Su, D.; Stach, E. A.; Ross, F. M. *Nano Lett.* **2015**, *15* (3), 1654−1659.
(6) Clark, T. E.; Nimmatoori, P.; Lew, K.-K.; Pan, L.; Redwing, J. M.; Dickey, E. C. *Nano Lett.* **2008**, *8* (4), 1246−1252.
(7) Hui, H. Y.; de la Mata, M.; Arbiol, J.; Filler, M. A. *Chem. Mater.* **2017**, *29* (8), 3397−3402.
(8) Wu, Y.; Fan, R.; Yang, P. *Nano Lett.* **2002**, *2* (2), 83−86.
(9) Dayeh, S. A.; Wang, J.; Li, N.; Huang, J. Y.; Gin, A. V.; Picraux, S. T. *Nano Lett.* **2011**, *11* (10), 4200−4206.
(10) Hu, Y.; Churchill, H. O. H.; Reilly, D. J.; Xiang, J.; Lieber, C. M.; Marcus, C. M. *Nat. Nanotechnol.* **2007**, *2* (10), 622−625.
(11) Higginbotham, A. P.; Kuemmeth, F.; Larsen, T. W.; Fitzpatrick, M.; Yao, J.; Yan, H.; Lieber, C. M.; Marcus, C. M. *Phys. Rev. Lett.* **2014**, *112* (21), 216806.
(12) Lauhon, L. J.; Gudiksen, M. S.; Wang, D.; Lieber, C. M. *Nature* **2002**, *420* (6911), 57−61.
(13) Takahashi, Y.; Nagase, M.; Namatsu, H.; Kurihara, K.; Iwdate, K.; Nakajima, Y.; Horiguchi, S.; Murase, K.; Tabe, M. *Electron. Lett.* **1995**, *31* (2), 136−137.
(14) Fujiwara, A.; Takahashi, Y.; Yamazaki, K.; Namatsu, H.; Nagase, M.; Kurihara, K.; Murase, K. *IEEE Trans. Electron Devices* **1999**, *46* (5), 954−959.
(15) Luo, Z.; Jiang, Y.; Myers, B. D.; Isheim, D.; Wu, J.; Zimmerman, J. F.; Wang, Z.; Li, Q.; Wang, Y.; Chen, X.; Dravid, V. P.; Seidman, D. N.; Tian, B. *Science* **2015**, *348* (6242), 1451−1455.
(16) Christesen, J. D.; Pinion, C. W.; Grumstrup, E. M.; Papanikolas, J. M.; Cahoon, J. F. *Nano Lett.* **2013**, *13* (12), 6281−6286.
(17) Geyer, N.; Huang, Z.; Fuhrmann, B.; Grimm, S.; Reiche, M.; Nguyenduc, T. K.; Boor, J. D.; Leipner, H. S.; Werner, P.; Gösele, U. *Nano Lett.* **2009**, *9* (9), 3106.
(18) Tersoff, J.; Jesson, D. E.; Tang, W. X. *Science* **2009**, *324* (5924), 236−238.
(19) Sutter, P.; Bennett, P. A.; Flege, J. I.; Sutter, E. *Phys. Rev. Lett.* **2007**, *99* (12), 125504.
(20) Hilner, E.; Zakharov, A. A.; Schulte, K.; Kratzer, P.; Andersen, J. N.; Lundgren, E.; Mikkelsen, A. *Nano Lett.* **2009**, *9* (7), 2710−2714.
(21) Wen, C. Y.; Reuter, M. C.; Bruley, J.; Tersoff, J.; Kodambaka, S.; Stach, E. A.; Ross, F. M. *Science* **2009**, *326* (5957), 1247.
(22) Perea, D. E.; Li, N.; Dickerson, R. M.; Misra, A.; Picraux, S. T. *Nano Lett.* **2011**, *11* (8), 3117−3122.
(23) Geaney, H.; Mullane, E.; Ramasse, Q. M.; Ryan, K. M. *Nano Lett.* **2013**, *13* (4), 1675.

DOI: 10.1021/acs.nanolett.8b02847
Nano Lett. 2018, 18, 6931−6940

(24) Flynn, G.; Ramasse, Q. M.; Ryan, K. M. *Nano Lett.* **2016**, *16* (1), 374−380.
(25) Lu, X.; Mata, M. D. L.; Arbiol, J.; Korgel, B. A. *Chem. Mater.* **2017**, *29*, 9786.
(26) Zakharov, N. D.; Werner, P.; Gerth, G.; Schubert, L.; Sokolov, L.; Gösele, U. *J. Cryst. Growth* **2006**, *290* (1), 6−10.
(27) Day, R. W.; Mankin, M. N.; Gao, R.; No, Y. S.; Kim, S. K.; Bell, D. C.; Park, H. G.; Lieber, C. M. *Nat. Nanotechnol.* **2015**, *10* (4), 345−352.
(28) Day, R. W.; Mankin, M. N.; Lieber, C. M. *Nano Lett.* **2016**, *16* (4), 2830−2836.
(29) Wolf, S.; Tauber, R. N. *Silicon Processing for the VLSI Era, Vol. 1*; Process Technology, 1986; Vol. *526*.
(30) Sze, S. M. *Physics of Semiconductor Devices*, 2nd ed.; Wiley: New York, 1981; Vol. *1*.
(31) Yu, L.; Alet, P.-J.; Picardi, G.; Roca i Cabarrocas, P. *Phys. Rev. Lett.* **2009**, *102* (12), 125501.
(32) Yu, L.; Roca i Cabarrocas, P. *Phys. Rev. B: Condens. Matter Mater. Phys.* **2009**, *80* (8), 085313−5.
(33) Yu, L.; Roca i Cabarrocas, P. *Phys. Rev. B: Condens. Matter Mater. Phys.* **2010**, *81* (8), 085323.
(34) Yu, L.; Xu, M.; Xu, J.; Xue, Z.; Fan, Z.; Picardi, G.; Fortuna, F.; Wang, J.; xu, j.; Shi, Y.; Chen, K.; Roca i Cabarrocas, P. *Nano Lett.* **2014**, *14*, 6469−6474.
(35) Xu, M.; Xue, Z.; Wang, J.; Zhao, Y.; Duan, Y.; Zhu, G.; Yu, L.; Xu, J.; Wang, J.; Shi, Y.; Kunji, C.; Roca i Cabarrocas, P. *Nano Lett.* **2016**, *16* (12), 7317−7324.
(36) Xue, Z.; Xu, M.; Zhao, Y.; Wang, J.; Jiang, X.; Yu, L.; Wang, J.; Xu, J.; Shi, Y.; Chen, K.; Roca i Cabarrocas, P. *Nat. Commun.* **2016**, *7*, 12836.
(37) Xu, M.; Wang, J.; Xue, Z.; Wang, J.; Feng, P.; Yu, L.; Xu, J.; Shi, Y.; Chen, K.; Roca i Cabarrocas, P. *Nanoscale* **2017**, *9*, 10350.
(38) Xue, Z.; Sun, M.; Dong, T.; Tang, Z.; Zhao, Y.; Wang, J.; Wei, X.; Yu, L.; Chen, Q.; Xu, J.; Shi, Y.; Chen, K.; Roca i Cabarrocas, P. *Nano Lett.* **2017**, *17* (12), 7638−7646.
(39) Xu, M.; Xue, Z.; Yu, L.; Qian, S.; Wang, J.; Xu, J.; Shi, Y.; Chen, K. J.; Roca i Cabarrocas, P. *Nanoscale* **2015**, *7*, 5197−5202.
(40) Yu, L.; Chen, W.; O'Donnell, B.; Patriarche, G.; Bouchoule, S.; Pareige, P.; Rogel, R.; Salaun, A. C.; Pichon, L.; Roca i Cabarrocas, P. *Appl. Phys. Lett.* **2011**, *99* (20), 203104−3.
(41) Tsang, J. C.; Mooney, P. M.; Dacol, F.; Chu, J. O. *J. Appl. Phys.* **1994**, *75* (12), 8098−8108.
(42) Dismukes, J.; Ekstrom, L.; Paff, R. *J. Phys. Chem.* **1964**, *68* (10), 3021−3027.
(43) Dismukes, J. P.; Ekstrom, L.; Paff, R. J. *J. Phys. Chem.* **1964**, *68* (10), 3021−3027.
(44) Nonnenmacher, M.; O'Boyle, M. P.; Wickramasinghe, H. K. *Appl. Phys. Lett.* **1991**, *58* (25), 2921−2923.
(45) Lu, W.; Xiang, J.; Timko, B. P.; Wu, Y.; Lieber, C. M. *Proc. Natl. Acad. Sci. U. S. A.* **2005**, *102* (29), 10046−10051.
(46) Chen, W.; Yu, L.; Misra, S.; Fan, Z.; Pareige, P.; Patriarche, G.; Bouchoule, S.; Cabarrocas, P. R. i. *Nat. Commun.* **2014**, *5*, 4134.
(47) Liscio, A.; Palermo, V.; Müllen, K.; Samorì, P. *J. Phys. Chem. C* **2008**, *112* (44), 17368−17377.
(48) Renner, O.; Zemek, J. *Czech. J. Phys.* **1973**, *23* (11), 1273.
(49) Kühnle, J.; Bergmann, R. B.; Werner, J. H. *J. Cryst. Growth* **1997**, *173* (1−2), 62−68.
(50) Thurmond, C. D. *J. Phys. Chem.* **1953**, *57* (8), 827−830.
(51) Fleurial, J. P.; Borshchevsky, A. *J. Electrochem. Soc.* **1990**, *137* (9), 2928−2937.

DOI: 10.1021/acs.nanolett.8b02847
Nano Lett. 2018, 18, 6931−6940